Supplementary Information for:

Tunable solid-state thermal rectification by asymmetric nonlinear radiation

Junbyeong Lee[1†], Agha Aamir Jan[1†], Shraddha Prakash Ganorkar [1†], Jungwan Cho[1],

Dongwoo Lee[1]*, and Seunghyun Baik[1]*

[1] School of Mechanical Engineering, Sungkyunkwan University, Suwon 16419, Republic of

Korea.

[†]These authors contributed equally to this work.

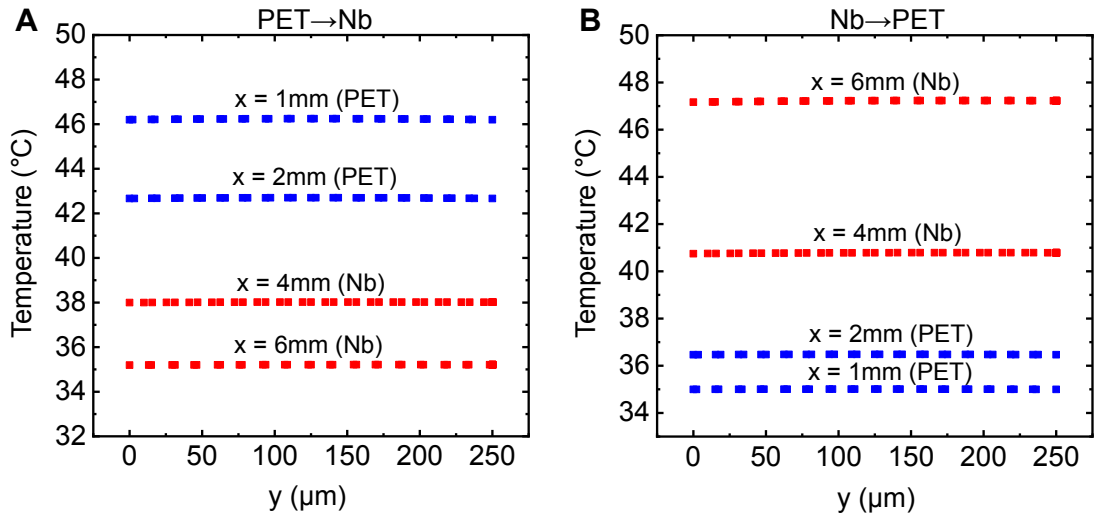*Corresponding author. Email: dongwoolee@skku.edu, sbaik@skku.edu

Fig. S1. The FEM analysis of the vertical temperature profile at x = 1, 2, 4, and 6 mm. The heat transfer mode is the combined conduction and radiation (constant heat flux boundary condition: 600 μW). (**A**) The heat transfer direction is from the PET side to the Nb side. The end temperatures are $T_{PET} = 50.9\ °C$ and $T_{Nb} = 33.9\ °C$. (**B**) The heat transfer direction is from the Nb side to the PET side. The end temperatures are $T_{PET} = 33.9\ °C$ and $T_{Nb} = 53.4\ °C$.
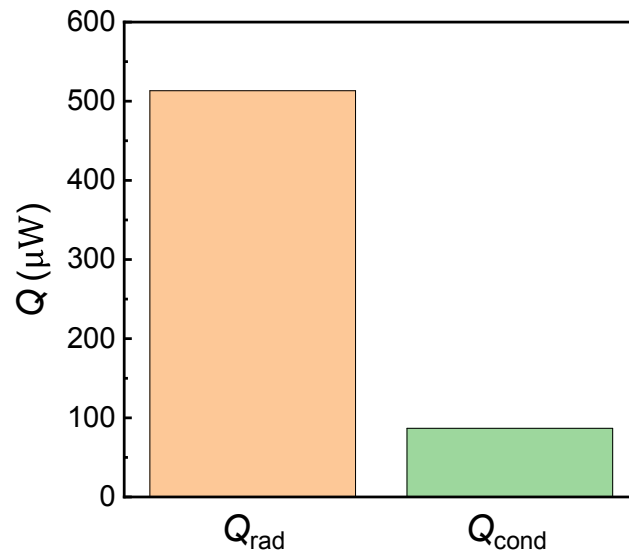
Fig. S2. The comparison of Q_{rad} and Q_{cond} calculated by FEM simulation. The forward heat flow (PET→Nb) and constant heat flux boundary condition (600 µW, T_L=33.9 °C, T_∞ = 30.9 °C) were considered.

A

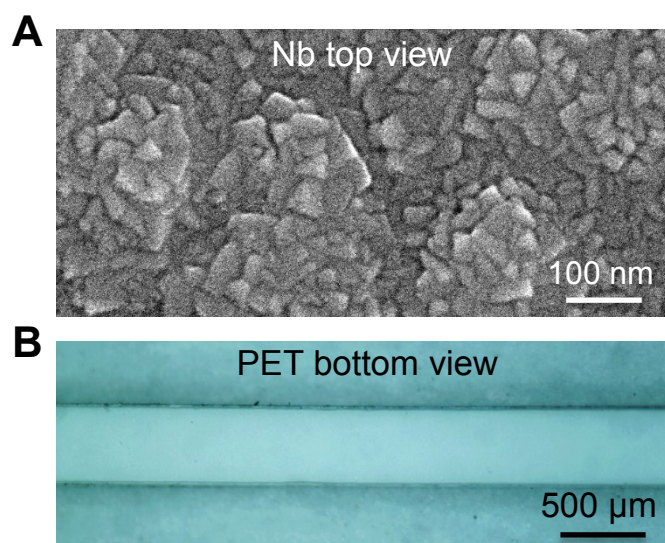Nb top view

100 nm

B

PET bottom view

500 µm

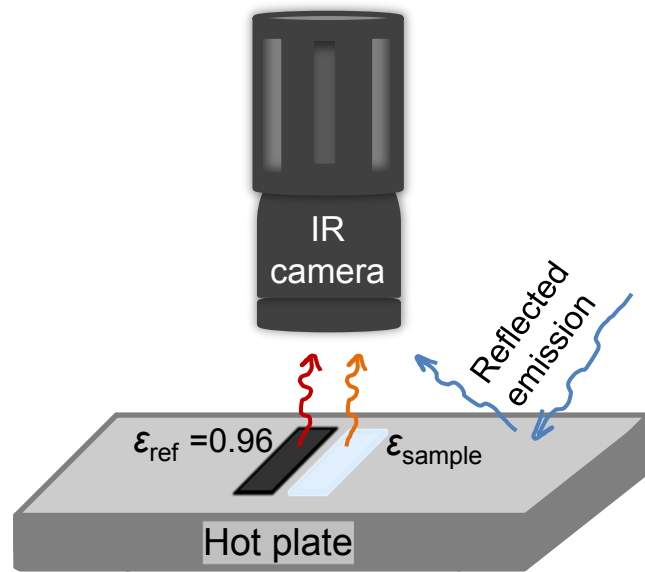**Fig. S3. The SEM image (top view of the Nb film) and optical image (bottom view) of the PET-Nb specimen.**

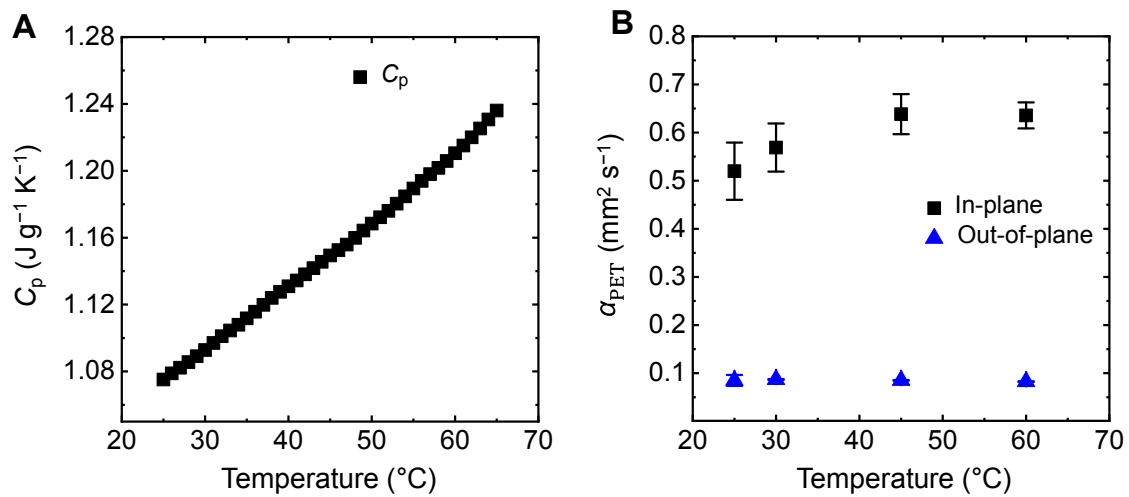**Fig. S4. The reflected temperature and emissivity calibration setup.**

Fig. S5. The specific heat and thermal diffusivity of the PET substrate.
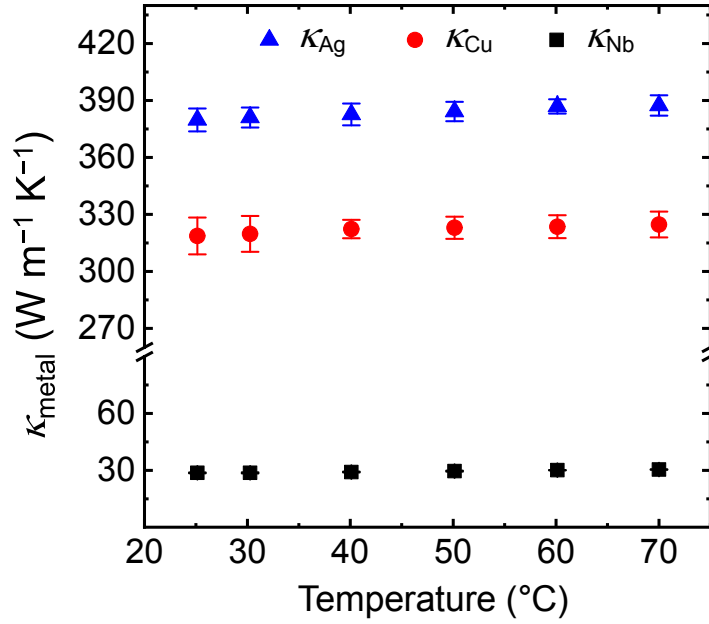
Fig. S6. The thermal conductivity of the Ag, Cu, and Nb films. The electrical conductivity of each metal film is experimentally measured as a function of the temperature by the four-point probe in-line method using a laboratory-built device[1]. The thermal conductivity (κ) is then obtained by $\kappa = \sigma L T$ (Wiedemann-Franz Law), where σ is the electrical conductivity, L is the Lorenz number, and T is the absolute temperature[2]. The Lorenz number for each metal is obtained from literature ($L_{Ag} = 2.31 \times 10^{-8}$ W Ω K^{-2}, $L_{Cu} = 2.20 \times 10^{-8}$ W Ω K^{-2}, and $L_{Nb} = 2.73 \times 10^{-8}$ W Ω K^{-2})[3,4]. The variation in κ is small in the investigated temperature range. The error bars represent the standard deviation of the data.
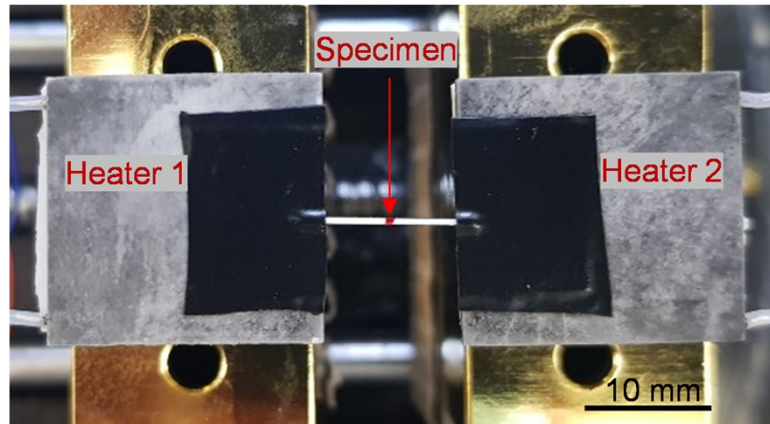
Fig. S7. An optical image (top view) of the PET-Nb specimen suspended between two ceramic heaters. The Nb film is facing down, and the top surface is PET. The specimen is firstly attached on the heaters using thermally conductive copper adhesive tape. The black tape is then placed on top of the copper tape to minimize reflection. The red arrow indicates the interface between the PET and Nb film which is on the bottom right side of the specimen.
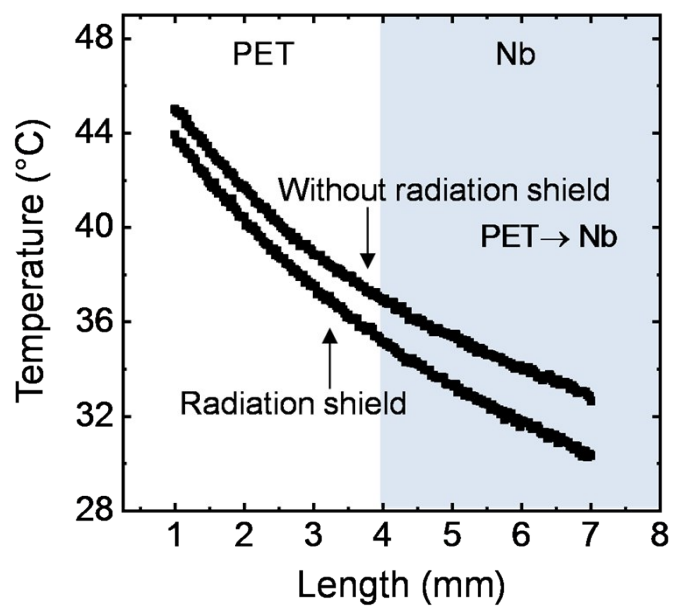
Fig. S8. The temperature profiles of the PET-Nb specimen with and without the radiation shield.
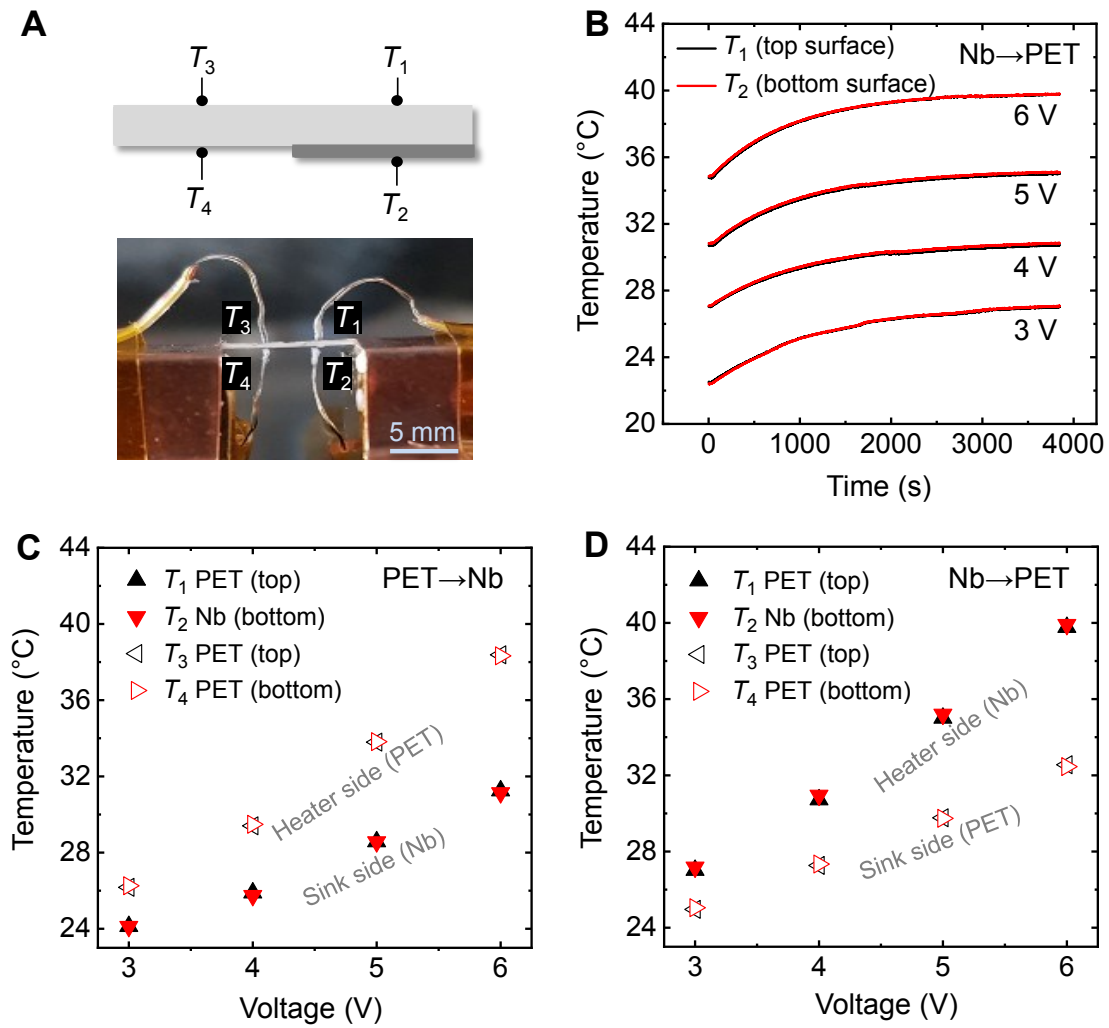
Fig. S9. The uniform temperature along the vertical *y*-direction of the PET-Nb specimen.
(**A**) The schematic and optical image of the top and bottom surface temperature measurement
setup using thermocouples. (**B**) The top (T_1) and bottom (T_2) surface temperatures increase as
the heater is turned on at each voltage. The steady state is reached after ~3600 s. (**C, D**) The
steady state temperatures (T_1, T_2, T_3 and T_4) for the forward and reverse heat transfer directions
are shown. There is negligible temperature difference between the top and bottom surfaces. The
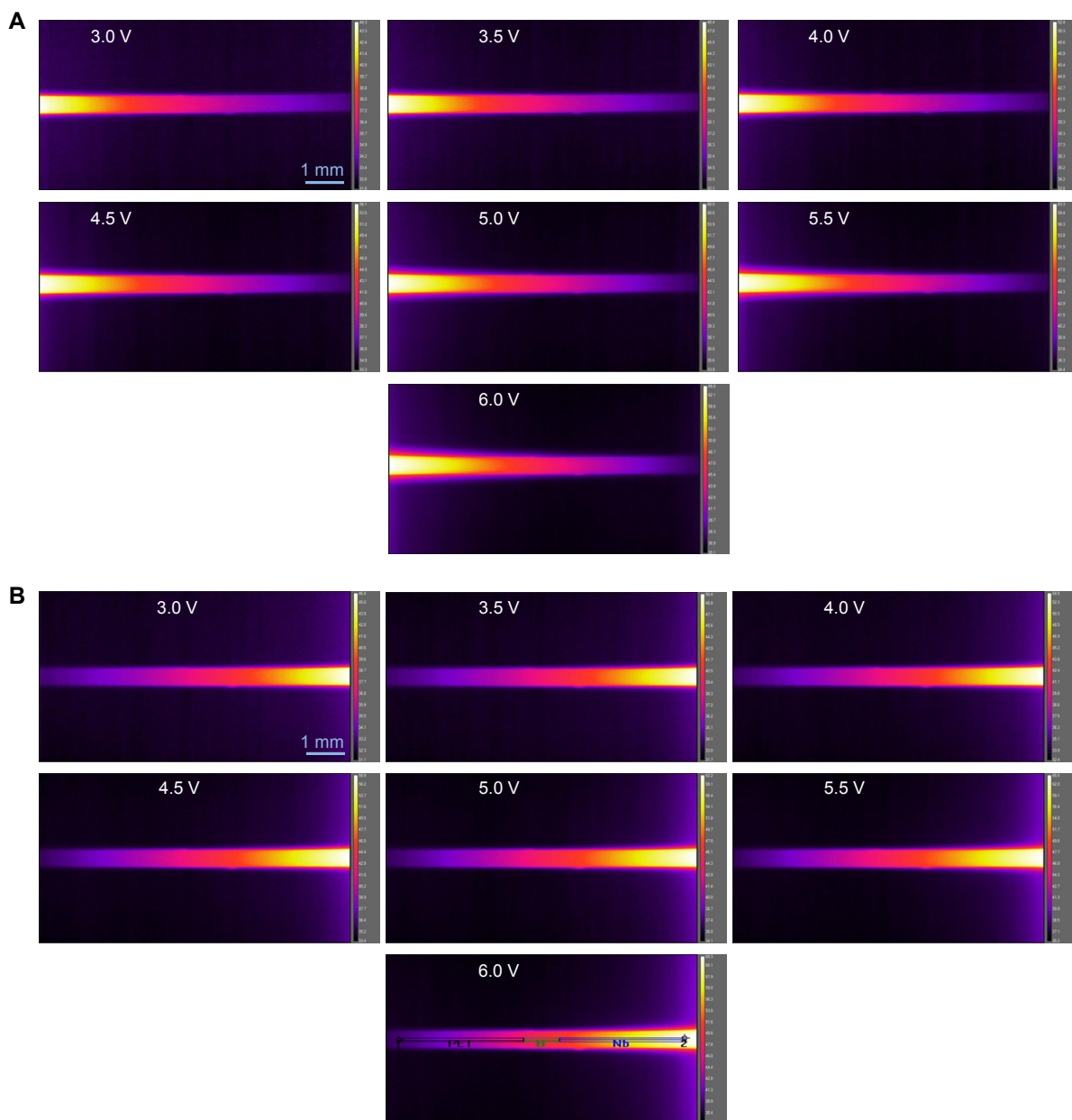heat transfer direction is designated by an arrow.

A

3.0 V

3.5 V

4.0 V

1 mm

4.5 V

5.0 V

5.5 V

6.0 V

B

3.0 V

3.5 V

4.0 V

1 mm

4.5 V

5.0 V

5.5 V

6.0 V

Fig. S10. The infrared images of the PET-Nb specimen. The applied heater voltage is shown. (**A**) The heat transfer direction is from the PET side to the Nb side. (**B**) The heat transfer direction is from the Nb side to the PET side.
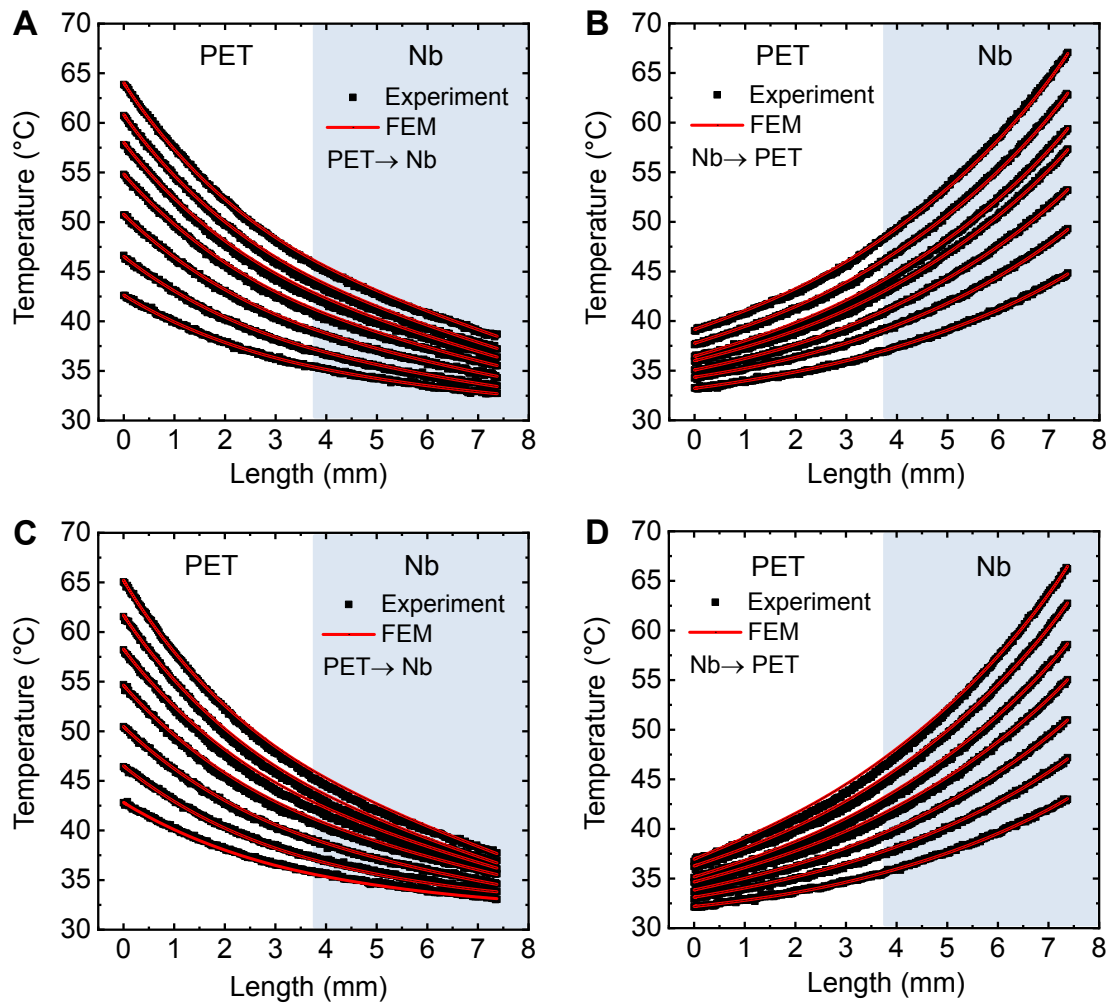
Fig. S11. The comparison of the experimental data and FEM analysis of the PET-Nb specimens at applied heater voltages between 3 and 6 V (0.5 V increment). Three specimens are investigated to demonstrate reproducibility. The experimental conditions are identical to those of the first specimen (Figs. 3C and D). The arrow indicates the heat transfer direction. (**A, B**) The second specimen data. (**C, D**) The third specimen data.
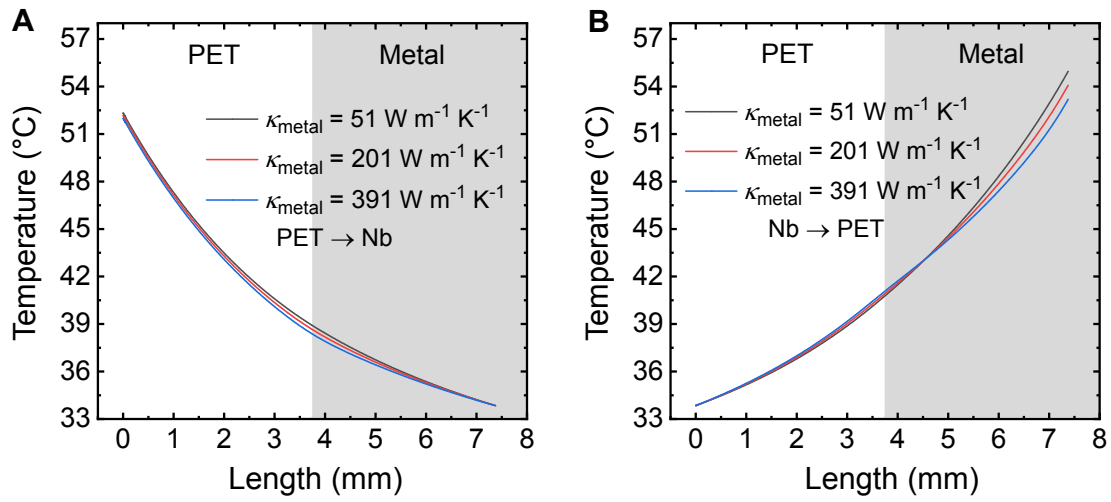
Fig. S12. The FEM analysis of the PET-metal specimens. The simulation is carried out using three different metal thermal conductivities (κ_{metal} = 51, 201 and 391 W m^{-1} K^{-1}) under a constant heat flux boundary condition (650 μW). The emissivity of metal is identical to that of Nb ($\varepsilon_{metal} = \varepsilon_{Nb}$). (**A**) The heat transfer direction is from the PET side to the metal side. (**B**) The heat transfer direction is from the metal side to the PET side.
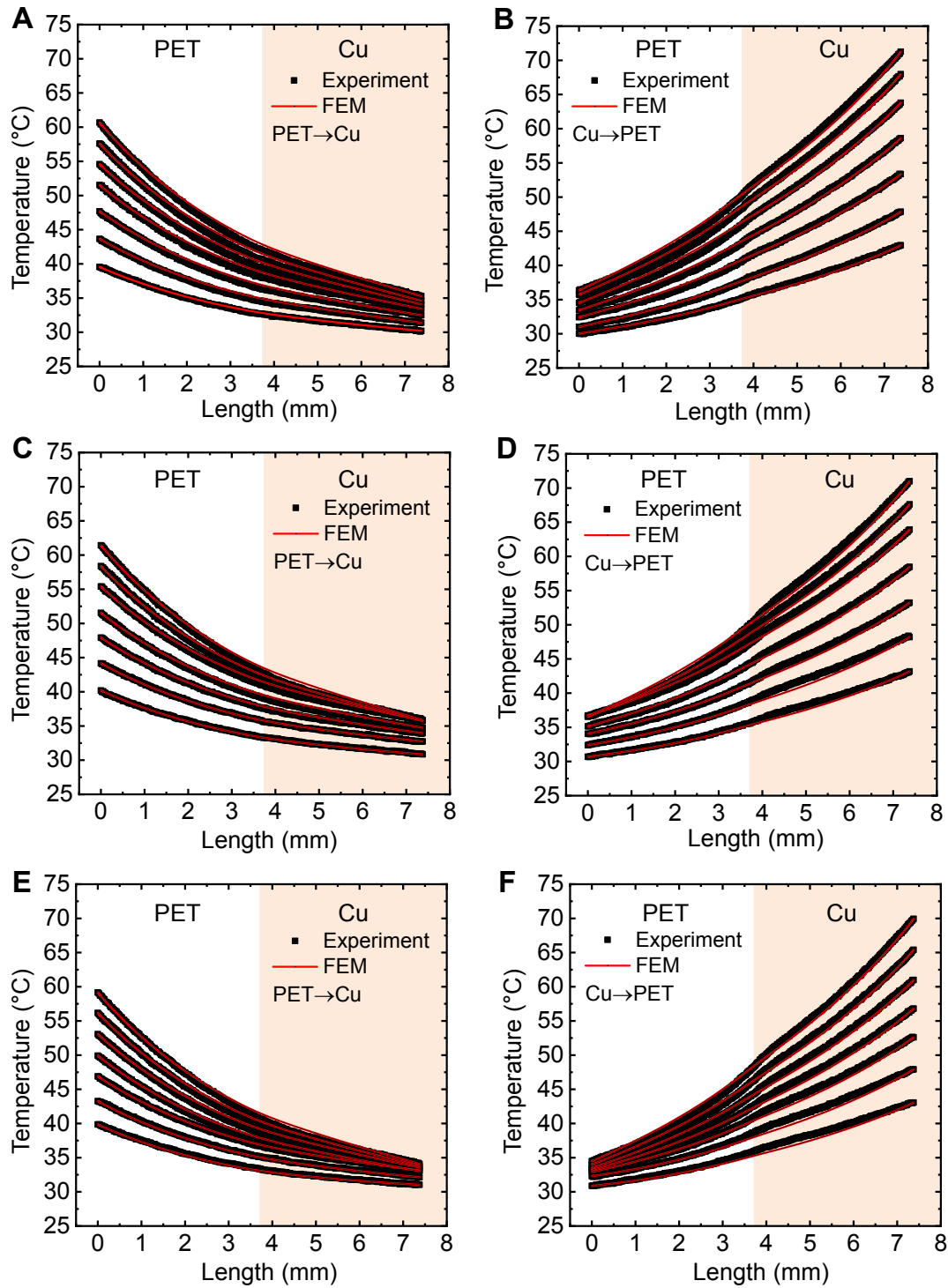
Fig. S13. The comparison of the experimental data and FEM analysis of the PET-Cu specimens at applied heater voltages between 3 and 6 V (0.5 V increment). Three specimens are investigated to demonstrate reproducibility. The arrow indicates the heat transfer direction. (**A, B**) The first specimen data. (**C, D**) The second specimen data. (**E, F**) The third specimen data.
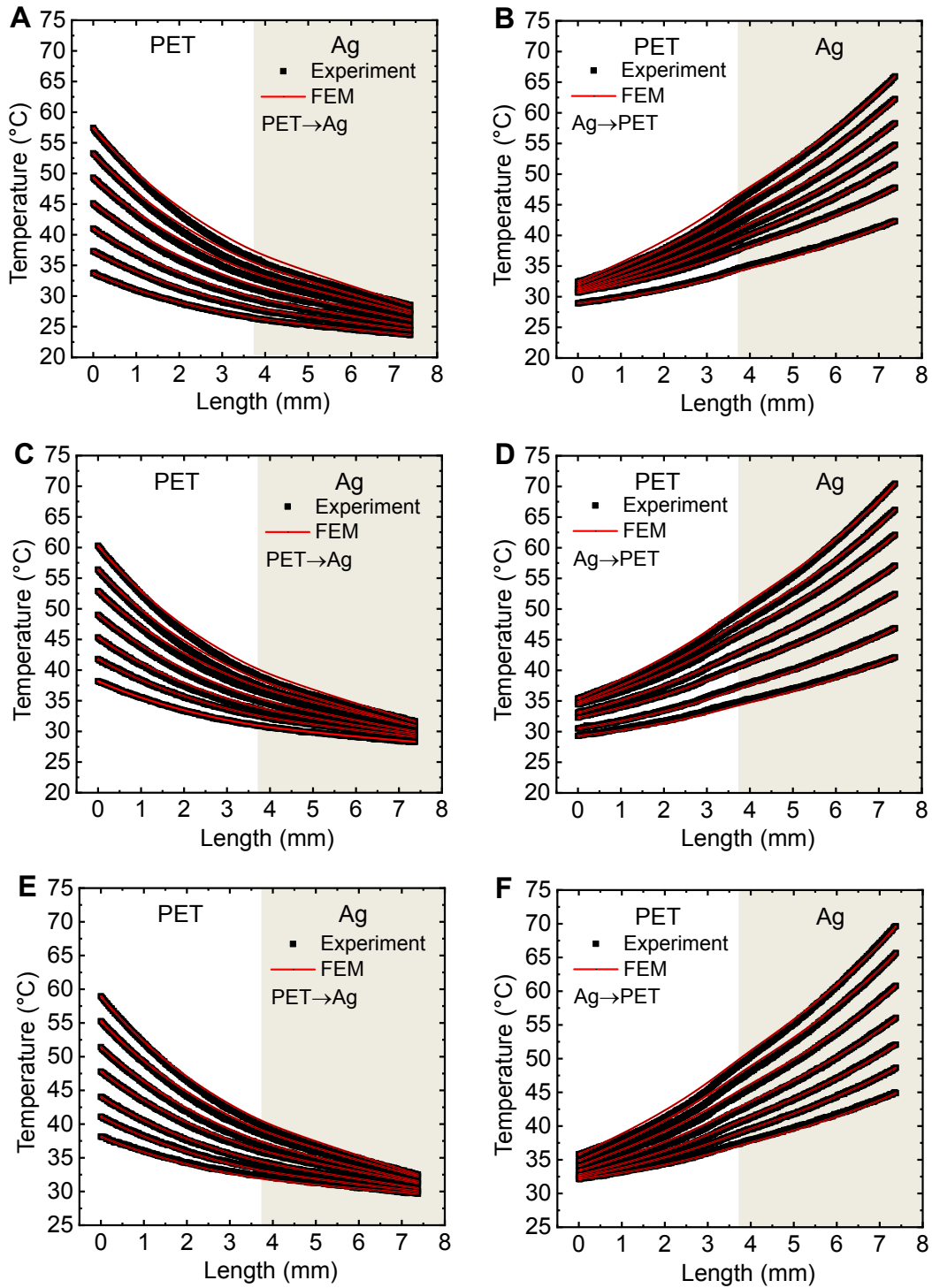
Fig. S14. The comparison of the experimental data and FEM analysis of the PET-Ag specimens at applied heater voltages between 3 and 6 V (0.5 V increment). Three specimens are investigated to demonstrate reproducibility. The arrow indicates the heat transfer direction. (**A, B**) The first specimen data. (**C, D**) The second specimen data. (**E, F**) The third specimen data.
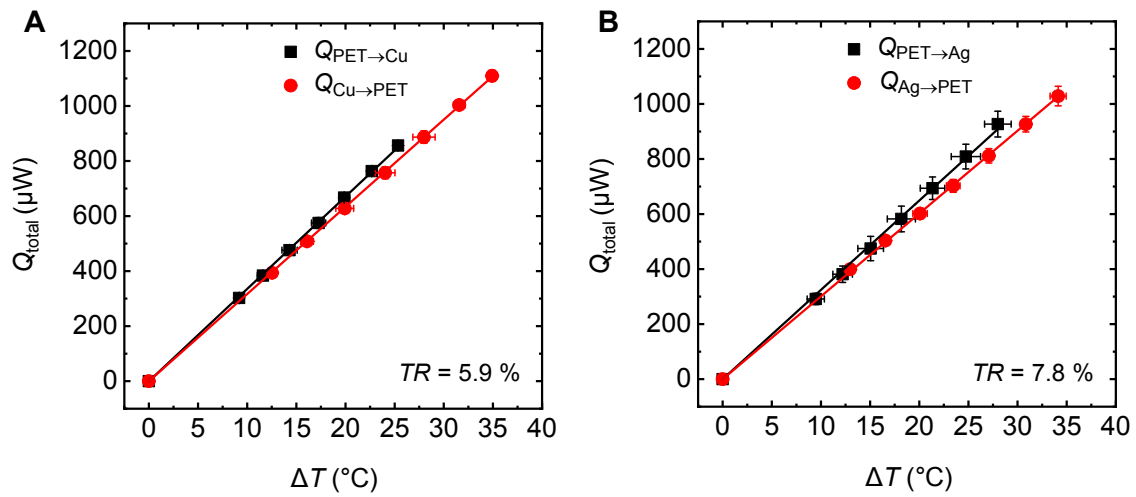
15

Fig. S15. The Q_{total} is shown as a function of the temperature difference between two ends (ΔT). The thermal rectification ratio is also shown at the bottom. The error bars represent the standard deviation of the data. (**A**) PET-Cu specimen. (**B**) PET-Ag specimen.
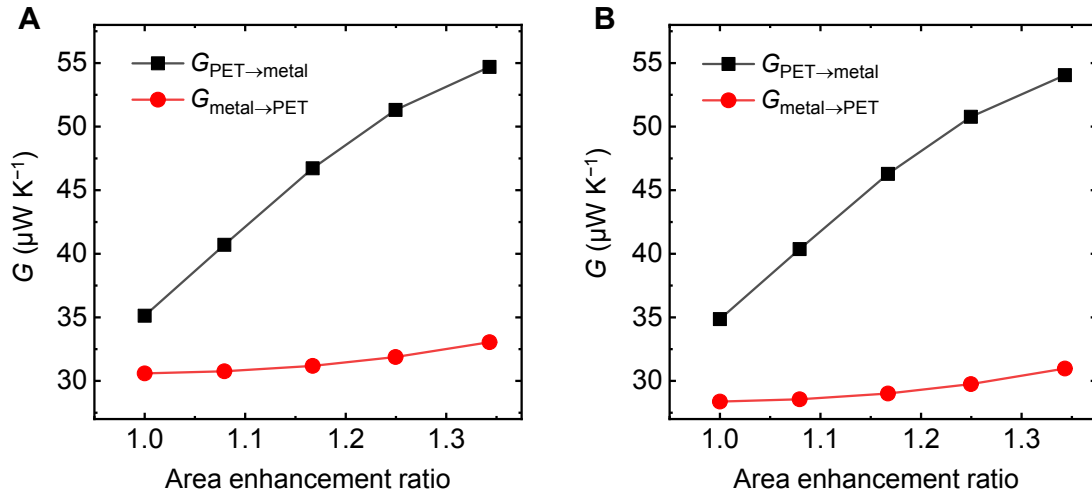
Fig. S16. The thermal conductances in forward and reverse directions are shown as a function of the area enhancement ratio. The thermal conductivity of metal is similar with that of Nb ($\kappa_{\text{metal}} = 28.8$ W m^{-1} K^{-1}). (**A**) The emissivity of metal is identical to that of Nb ($\varepsilon_{\text{metal}} = \varepsilon_{\text{Nb}}$). (**B**) $\varepsilon_{\text{metal}} = 0.1$.
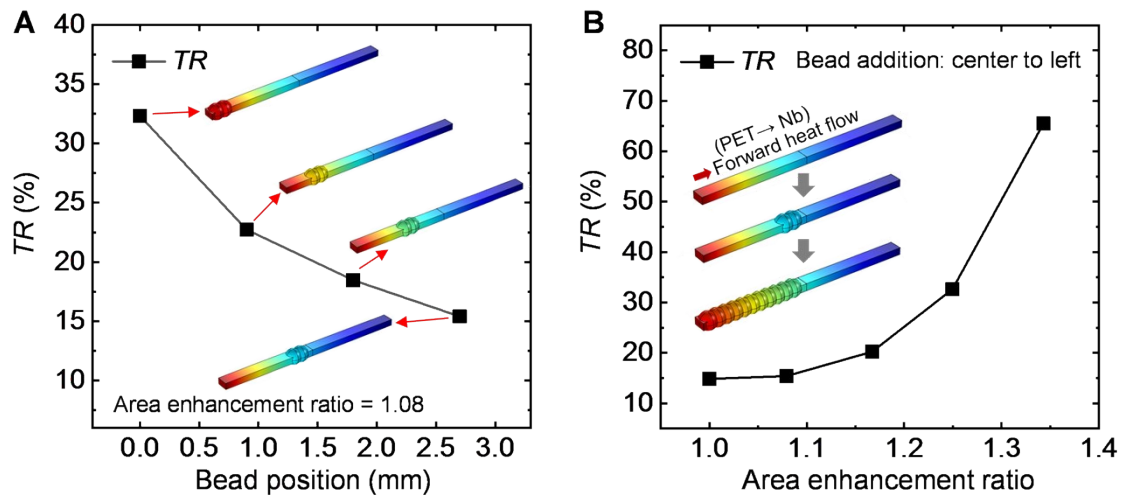
Fig. S17. The thermal rectification ratio of the PET-Nb specimen is calculated by FEM simulation. The corresponding geometry with bead-shaped surface (PET side) is provided in the inset. The simulation is carried out using a constant heat flux boundary condition (650 μW, $T_L = 33.9$ °C, $T_\infty = 30.9$ °C). **(A)** The bead-shaped surface is constructed at different positions. The area enhancement ratio is identical (1.08). **(B)** The bead-shaped surface is added from the center to the left high-temperature end.

References

1.   Suh, D., Moon, C. M., Kim, D. & Baik, S. Ultrahigh Thermal Conductivity of Interface Materials by Silver-Functionalized Carbon Nanotube Phonon Conduits. *Adv. Mater.* **28**, 7220–7 (2016).

2.   Balandin, A. A. Thermal properties of graphene and nanostructured carbon materials. *Nat. Mater.* **10**, 569–581 (2011).

3.   N. W. Ashcroft; N. D. Mermin. *Solid State Physics* (Saunders College Publishing, New York 1976).

4.   Raag, V. & Kowger, H. V. Thermoelectric properties of niobium in the temperature range 300°-1200°K. *J. Appl. Phys.* **36**, 2045–2048 (1965).